Considering Density Functional Approaches for Actinide Species: The An66 Molecule Set

Lucas E. Aebersold and Angela K. Wilson*

Department of Chemistry, Michigan State University, East Lansing, Michigan 48824-1322, United States

E-mail: akwilson@msu.edu

This document is the Accepted Manuscript version of a Published Work that appeared in final form in the Journal of Physical Chemistry A 125(32), 7029-7037 (2021), copyright © 2021 American Chemical Society after peer review and technical editing by the publisher. To access the final edited and published work see http://pubs.acs.org/articlesonrequest/AOR-UBV5EWZUZBGBUVGWZ8Z5.

Publication Date: August 9, 2021
DOI: https://doi.org/10.1021/acs.jpca.1c06155

Abstract

The importance of spin-orbit effects on the predictions of energetic properties of actinide compounds has been considered for eighteen different density functionals, comparing the spin-orbit and non-spin-orbit ("standard") forms of density functional theory (DFT) A set of enthalpies of formation for 66 small actinide (Th-Am) compounds, the An66 set, for which experimental data is available—have been investigated. The set includes actinide halides, oxides and oxohalides in the general form AnO_mX_n, where $n = 0 - 6,\ m = 0 - 3$, and X = F, Cl, Br, or I. The impact of basis set choice was investigated, and, to help account for the impact of relativity, the Stuttgart general and segmented contracted atomic natural orbital (ANO) basis sets paired with small core relativistic effective core potentials (RECP), as well as all-electron calculations utilizing the third-order Douglas-Kroll-Hess were considered.

Introduction

Actinide compounds are of interest in many applications, with the use of actinide oxides in nuclear fuel cycles being one of the most common.[1,2] Other applications in medicine, energy production and catalysis are widespread, and include actinide use in cancer therapy, smoke detectors, heart pacemakers, power sources, missiles, and actinide-doped materials to achieve properties such as luminescence. While there are many uses of actinides, there are also significant ongoing environmental challenges, in terms of the nuclear waste generated as a byproduct towards its many applications. Transuranic elements, which contribute the most heat to underground storage facilities, have half-lives on the order of tens-to-ten thousands of years. Separating these species from the waste makes their transmutation into species that decay much faster more feasible and also facilitates potential reuse.[3] Thermochemistry is an essential key to the nuclear separation process, the design of new actinide-based catalysts and applications, and improvement of existing processes.

In addressing actinide species, computational chemistry provides a vital route towards

describing their thermochemistry, in part, due to the inherent difficulties of experimental work with such compounds.[4] However, computational methods have their own challenges. Calculations on f-block species are inherently difficult due to the preponderance of nearly-degenerate states, the influence of relativistic effects, and the need to account for high levels of electron correlation, which all pose significant demands on electronic structure methods. Combining the methodological requirements for f-block species makes even small molecule calculations costly in terms of computer time, memory, and disk space.

There are several routes that can be used to account for relativistic effects, with Hamiltonians that incorporate various levels of relativistic effects. One of the most accurate methods for the treatment of relativistic effects is the four-component Dirac-Hartree-Fock (DHF) method. A drawback of the method, however, is that it is computationally demanding, largely restricted to very small molecules, and careful analysis is required to collect meaningful results. More approximate two-component methods such as Douglas-Kroll-Hess (DKH) and zeroth-order regular approximation (ZORA) allow the inclusion of effects such as scalar relativistic contraction and spin-orbit coupling, while enabling a significant reduction of computational effort relative to DHF-based approaches.

As molecule size increases, even these approximate methods can become too computationally costly, and instead, scalar relativistic corrections are considered in a one-component representation, incorporating effects of relativity within relativistic effective core potentials (RECPs).[5] These Hamiltonians can be used with standard wavefunction based methods and density functional based methods. As molecules get bigger in terms of the number of electrons, the computational cost soars. Thus, rather than using ab initio methods (CCSD, MRCC, etc.) Kohn-Sham density function approaches become more favorable. This is especially the case for heavy elements due to the efficiency of DFT approaches relative to *ab initio* approaches, enabling molecules of larger size to be investigated, while accounting for electron correlation.

Most density functional approaches, however, were designed for the study of main group species, largely with parameterization based upon properties of main group species, with

only a limited number of functionals incorporating any transition metal chemistry data in their parameterization, and, of those, very little transition metal data is used. This suggests that significant examination of property prediction be done to help ensure the utility and relevance of the functionals in this regime of the periodic table.

In considering a broad perspective of functional performance across the periodic table, for main group energetics, overall, the root mean square deviation of over 1,000 energies from experiment is ∼2–4 kcal mol^{-1}, generally depending upon functional class.[6] For $3d$ transition metals, this deviation increases, overall, so that the best functionals for a set of ∼200 enthalpies of formation different from experiment with a root mean squared deviation (RMSD) of 6–9 kcal mol^{-1}. It is important to note as well, however, that reported experimental uncertainties for these different energy sets also increase across the periodic table.[7,8] Nevertheless, there is still a need to take stake of the performance.

In recent work on the lanthanides, it was observed that overall, there is a deviation in the enthalpies of formation and dissociation energies for the Ln54 set, a set of 54 lanthanide energies from experiment, of ∼1 eV.[7,9] This is a sizable error, especially considering the small molecules that were investigated. While there are *ab initio* methods that markedly reduce this error, the computational demands can quickly become daunting. In the present study, the impact of functional and basis set choice, as well as the impact of spin-orbit effects, on the energy predictions for actinides, is considered.

Computational Methods

Density functional calculations were performed on a set of actinide compounds and their constituent atoms. The actinides chosen are based on our compilation of 66 actinide energies from experiment—which we call the An66 set. 18 commonly used functionals were used, representing several families of functionals, some of which have performed the best in prior DFT studies of transition metal or lanthanide species, including: the local spin density approximation

(LSDA) SVWN[10,11]; the generalized gradient approximations (GGA) [BP86,[12,13] BLYP,[12,14] PW91,[15] and PBE[16]]; meta-corrected GGAs (mGGAs) [TPSS[17] and M06-L[18]]; a variety of hybrid GGAs with various levels of exact exchange [B3P86,[13,19] X3LYP,[11,12,14,15] B97-1,[20,21] B3LYP,[14,19] PBE0,[22] MPW1K,[23] BHLYP[14,19]]; meta-hybrids [TPSSH,[24] M06[25] and M06-2X[25]]; and the double hybrid functional B2PLYP.[26,27] All calculations were performed with the NWChem[28] computational suite of software.

The effects of all-electron methods and relativistic effective core potential methods were analyzed. For the RECP calculations, three basis sets from the Stuttgart family of RECPs were considered for each actinide atom. All RECP basis sets used the same small core pseudopotential fit to the quasi-relativistic Wood-Boring results for many electrons (ECP60MWB).[29–31] The first basis set, the Stuttgart 1997 RSC (S97) is a $(12s11p10d8f)/[8s7p6d4f]$ segmented contracted basis set, that is less demanding computationally with respect to other commonly used RECP basis.[30] However, as noted by Cao et al.[30] the basis set has specific drawbacks. Thus, for geometry optimization the $(14s13p10d8f6g)/[6s6p5d4f3g]$ segmented contracted atomic natural orbital (SEG) basis, given by Cao and co-workers[32] was used for all actinide compounds.

Additionally, the pVQZ quality $(14s13p10d8f6g)/[6s6p5d4f3g]$ general contracted atomic natural orbital (ANO) basis[30] was used for single point energies. For the lighter ligands O, F, Cl the cc-pVTZ basis sets (cc-pV(T+d)Z for Cl) were used.[33,34] For the heavier ligands Br and I, relativistic effects should be addressed, thus the small-core Stuttgart-Köln ECP10MDHF and ECP28MDHF pseudopotentials with the cc-pVTZ-PP basis sets were employed.[35]

Geometry optimization was performed with the TPSS[17] meta-GGA functional using the unrestricted Kohn-Sham formalism. The TPSS functional was selected, based on its effectiveness in systems with many degenerate states.[16,17,36] The optimized structures were used in the ANO and AE calculations. As such, optimizations with other basis sets were not considered. For molecules that have available experimentally determined states (i.e., actinide oxides), the DFT calculations were aligned with those states.[2] To determine the ground state

multiplicity of compounds with no experimental reference, calculations were done across a range of likely multiplicities and states. The orbital vectors were checked, and rotations done if needed to identify the lowest energy state possible. This state was used as the ground state for all calculations. Vibrational frequencies were calculated with NWChem's built in numeric methods, and no imaginary frequencies were present for the final optimized structures.

In prior studies on small lanthanides, in general, functional choice for the geometry optimization results in small differences in the overall prediction of the computed enthalpies of formation (considering the magnitude of error).[7,9] For example, in a previous DFT study of the lanthanides, structures optimized with SVWN, PBE, TPSS, M06-2X, and PBEO resulted in enthalpies of formation and bond dissociation energies that differed, largely by less than a single kcal mol^{-1}.[9] Thus, the structures optimized with TPSS were utilized in single-point calculations for all of the other functionals and basis sets for each compound.

Spin–orbit DFT (SO-DFT) calculations were performed using NWChem's SO-DFT method for the SEG and ANO basis with the small-core Stuttgart RECPs. For the all-electron calculations, the third-order Douglas-Kroll-Hess method,[37] as implemented in NWChem,[38] was used. The cc-pVTZ-DK basis sets[35,39,40] are used for of the all atoms. Third-order Douglas-Kroll-Hess was used as it has been shown to be more accurate than second-order DKH.[39,41,42] For the all-electron calculations, DKH and ZORA are common choices. Here, the DKH method was selected as prior work suggested ZORA and DKH have similar performance.[43]

To assess the predictive capability of the functionals, a set of experimental enthalpies of formation, ΔH_f^{298K}, for 66 actinide compounds was utilized (An66). The energies were taken from Nuclear Energy Agency (NEA)[44,45] data and a recent 2014 review/survey of actinide oxides.[46] The set of compounds includes a variety of oxides, halides, and oxohalides for actinides Th, U, Np, Pu, and Am. The thorium compounds included were: ThX_n where X = F, Cl, or Br, and n = 1–4, as well as ThO_n (n = 1,2),[46] ThOF, and ThI_4. For uranium the 26 compounds included were: UX_n where X = O (n = 1–3),[46] F (n = 1–6), Cl (n = 1–6), Br (n = 1–5), and I (n = 1–4). Additionally, the oxohalides UOF_4, UO_2F_2, and UO_2Cl_2 were

included. For neptunium 9 compounds included were NpX_n where X = F (n = 1–4, 6), Cl (n = 3, 4), and O (n = 1, 2).[46] Plutonium compounds consisted of PuX_n where X = F (n = 1–4, 6), Cl (n = 3, 4), Br (n = 3), I (n = 3), and O (n = 1–3).[46] Lastly, two Am compounds were considered AmO and AmF_3.

The enthalpies were computed using a thermodynamic cycle. Linear regression analysis of computed values versus experimental values, along with mean unsigned errors (MUE) and mean signed errors (MSE) were used to assess the performance of the functionals.

Results and Discussion

Enthalpies of Formation

To analyze the utility of the basis sets, the all-electron DKH3 basis, the generally contracted ANO RECP basis, the segmented contracted RECP basis, and 1997 Stuttgart RECP basis are compared using several different metrics. The error from the experiment value, that is, the computed value subtracted from the experimental value was taken for each compound. The mean signed errors (MSE) and mean unsigned errors (MUE) with respect to experiment were computed for the data set as a whole and also for subsets of the data. In addition, the minimum error (most negative), maximum error (most positive), and standard deviation are also reported. To attain a better idea of the overall consistency—the distribution of the error and accuracy of the energies across a span of molecules—of the functionals, linear regression statistics, including the R^2, slope and intercept values, were utilized. The analysis here was done by considering each subset of compounds—Th, U, and Np species, and a subset including Pu and Am compounds together due to the limited numbers of Am species.

For the actinide subsets, the MUEs in the energies for each functional and basis set are shown in Fig. 1. For the thorium compounds, the MUEs were the best overall, with values ranging from 5 to 10 kcal mol^{-1}, with the exception of SVWN, whose error is approximately 23 kcal mol^{-1} for each basis. Spin–orbit coupling does not drastically affect most of the thorium

Table 1: Statistical properties computed for the enthalpies predicted by each functional, for the SEG, ANO, and AE basis sets. The statistics include the mean unsigned error (MUE), mean signed error (MSE), the range of errors noted (Min and Max), all in kcal mol^{-1}, and finally the standard deviation σ.

	MUE			MSE			Min			Max			σ		
	SEG	ANO	AE	SEG	ANO	AE	SEG	ANO	AE	SEG	ANO	AE	SEG	ANO	AE
SVWN	25.2	23.2	25.1	−21.0	−18.3	−21.6	−90.3	−85.4	−96.6	25.2	22.8	21.7	20.7	19.5	21.4
BP86	12.0	10.7	12.1	0.2	2.4	−0.8	−35.4	−32.4	−41.9	43.3	39.5	39.3	10.2	9.7	10.5
BLYP	11.9	12.1	12.1	6.1	8.8	5.2	−25.8	−20.3	−33.2	46.1	41.8	41.8	11.1	11.1	10.9
PW91	12.9	11.3	12.8	−3.3	−1.0	−4.7	−42.9	−38.1	−50.1	39.6	35.2	34.9	10.4	9.8	11.3
PBE	12.6	11.2	12.3	−1.3	0.9	−2.6	−39.0	−35.3	−45.6	42.6	38.7	38.1	10.4	9.9	11.0
TPSS	11.0	9.2	14.9	−4.7	−2.4	−9.0	−41.0	−36.0	−46.8	33.4	26.4	29.8	8.8	7.9	10.4
M06-L	11.6	10.9	11.4	1.7	3.3	−2.9	−32.9	−29.1	−36.1	40.1	36.5	28.5	9.6	9.5	8.5
B3P86	11.9	11.4	13.0	−2.5	−0.2	−3.9	−21.9	−19.4	−28.6	33.1	32.0	29.0	7.2	7.9	7.8
X3LYP	11.6	12.0	11.6	3.9	6.4	2.6	−20.6	−17.3	−21.0	37.5	44.0	36.8	9.2	10.7	9.2
B97-1	11.6	12.1	13.1	2.7	4.7	1.5	−22.0	−19.3	−22.6	38.9	39.9	40.6	9.3	10.7	9.4
B3LYP	11.4	12.1	11.6	4.3	6.9	2.7	−20.4	−16.7	−20.8	37.9	45.7	34.7	9.4	11.1	9.2
PBE0	11.5	11.6	12.4	−0.2	2.9	−1.5	−21.1	−18.4	−24.3	35.3	40.8	36.2	8.6	9.9	8.3
MPW1K	12.7	13.6	13.5	0.5	3.3	−0.7	−21.6	−21.7	−26.0	53.3	60.0	54.4	9.7	12.2	10.6
BHLYP	14.9	16.3	15.3	6.0	9.0	5.5	−20.3	−17.4	−22.3	64.9	72.0	73.0	13.3	16.5	15.1
TPSSH	10.7	10.4	11.9	−4.8	−2.8	−6.4	−28.4	−23.6	−35.5	31.8	26.8	27.2	7.1	6.7	8.1
M06	17.0	17.6	12.8	13.1	15.0	5.9	−18.9	−12.6	−21.3	51.0	52.9	51.7	14.2	14.4	10.6
M06-2X	17.2	20.1	17.4	10.1	10.5	10.9	−21.6	−19.8	−26.0	84.1	90.8	72.6	18.5	20.8	19.3
B2PLYP	13.4	12.7	15.4	−2.5	1.1	−4.6	−41.0	−37.7	−51.4	35.7	58.6	60.4	8.9	10.4	12.5

species considered, likely due to the singlet nature of ThX_2, ThX_4, and ThO compounds—where X can be O, F, Cl, Br, and I. Other molecules in the set are doublets. There is also little difference arising from energies determined using the all-electron basis sets and the RECP basis sets.

The uranium compounds make up the majority of the An66 set and the trends exhibited are more complicated than for the thorium compounds. As shown in the lower left panel of Fig. 1, the MUEs for each functional and the respective basis set begin to diverge in the sense that there are substantial differences in the MUEs, depending upon functional. For example, the MUE of the TPSS functional is the highest at 19.6 kcal mol^{-1} for the AE basis set, yet the MUEs for the S97, SEG, and ANO are 12.7, 12.1, and 9.9 kcal mol^{-1}, respectively. An increase in the MUE for functionals with higher amounts of exact exchange occurs for all basis sets, such as B3LYP (23%), PBE0 (25%), to MPW1K (46%), to BHLYP (50%). However, the Minnesota functionals, M06 and M06-2X—which have 26 % and 54 % exact exchange, respectively—do not result in such an increase for uranium.

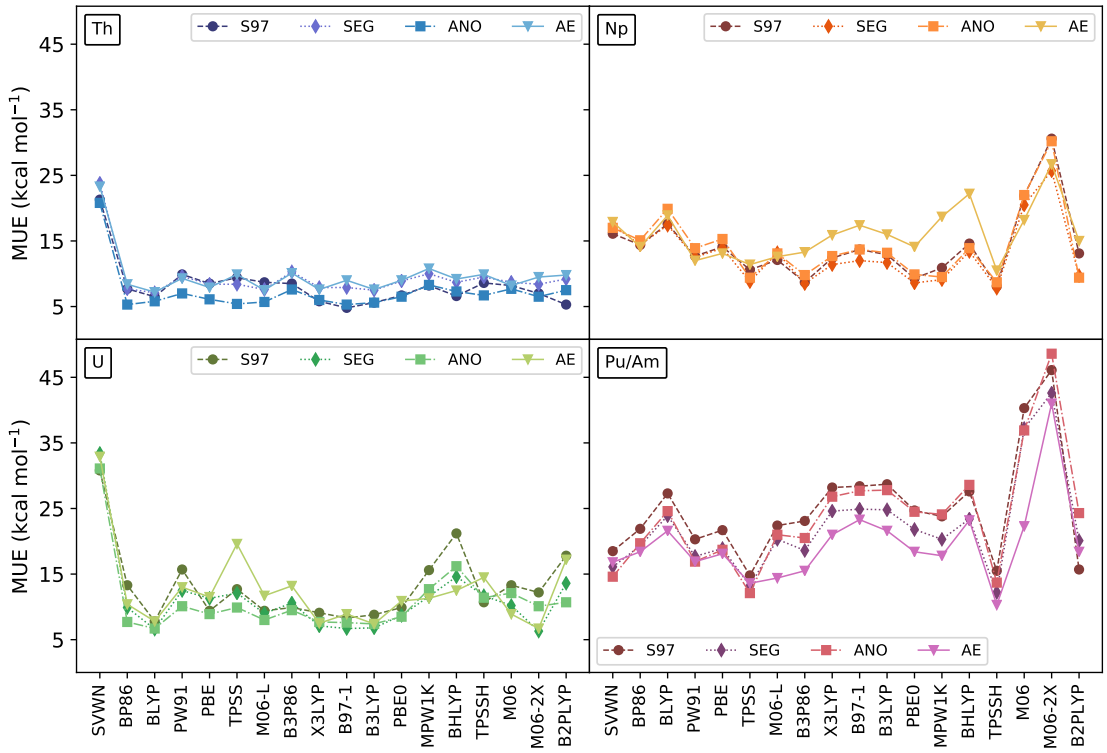

Figure 1: A comparison of functionals and the four basis sets, S97, SEG, ANO, and AE. MUEs for each actinide are given in the four panels in kcal mol^{-1}, the upper left shows the MUEs for all Th compounds. The lower left shows the MUEs for all U compounds, the upper right shows the results for the Np compounds and finally the lower right shows the combined MUE for the Pu and Am compounds.

Relative to the MUEs for uranium and thorium compounds, for neptunium compounds, there is an increase in the MUEs for nearly all functional and basis set selections. For the HGGAs MUEs are higher for the AE basis than for the RECP basis sets, but for the meta HGGAs this is not the case. The TPSSH functional results in the lowest MUEs of the functionals for all basis sets, with values of 8.1, 10.5, 7.8, and 8.7 kcal mol^{-1} for S97, AE, SEG, and ANO sets, respectively. The RECP MUE values of TPPSH are similar regardless of the RECP used. The large errors in energies for the SVWN functional observed for the uranium and thorium compounds are smaller for Np, with MUE's of $\sim$17 kcal mol^{-1}. To note, for thorium and uranium compounds, SVWN predicted far more negative enthalpies of formation than the other functionals and experiment. However, for Np, functionals other than SVWN result in MUEs that are higher than the experimental enthalpy. With SVWN's tendencies

to predict enthalpies that are more negative than for the other functionals, the resulting MUE is closer to experiment. The predictions arising from the Minnesota functionals, M06 and M06-2X, are not as good for the neptunium compounds as for uranium and thorium compounds, as most MUEs range from ∼20 to 30 kcal mol^{-1}.

For the plutonium and americium compounds, the MUE values are also large, and the differences arising from the basis sets choice are more evident. In contrast to the Np compounds, the AE basis set for nearly every functional results in the lowest MUE. Though the AE MUE values for Pu and Am are actually similar to the Np values, there is a large increase in the MUEs for the RECP basis sets. The TPSSH functional provides MUEs of 15.5, 10.3, 12.2 and 13.7 kcal mol^{-1} for the S97, AE, SEG, and ANO basis sets, respectively. The TPPSH values do not show much fluctuation across the plutonium and americium compounds, as for the SVWN and Minnesota (M06) functionals with exact exchange. The M06 and M06-2X functionals experience a large decrease in performance, having MUEs in the range of 40 to 50 kcal mol^{-1}, the highest of all functionals across the actinide series. Plutonium oxides are known to have significant multireference character,[47] which can be problematic for DFT approaches, in general, and as demonstrated for actinides by a prior study on AtO^+.[48] This may explain the particularly high MUEs observed, especially for the functionals with higher percentages of exact exchange. Prior studies have shown that higher percentages of exact exchange in functionals leads to poorer predictions of energetics for systems with significant multireference character.[7,48]

To give an overall summary of performance, the total MUEs for all compounds are given in Figure 2. In Table 1 the MUE, MSE, range (minimum and maximum), and the standard deviations for all of the enthalpies computed for the An66 set for each functional and the AE, SEG, and ANO basis sets are provided.

For the AE basis set, the lowest MUE is achieved by M06-L and B97-1 with values of 11.4 and 11.6 kcal mol^{-1}, respectively. The MSE for B97-1 was 1.5 kcal mol^{-1} while the MSE of M06-L was −2.9 kcal mol^{-1}, indicating that the enthalpy predictions did not strongly

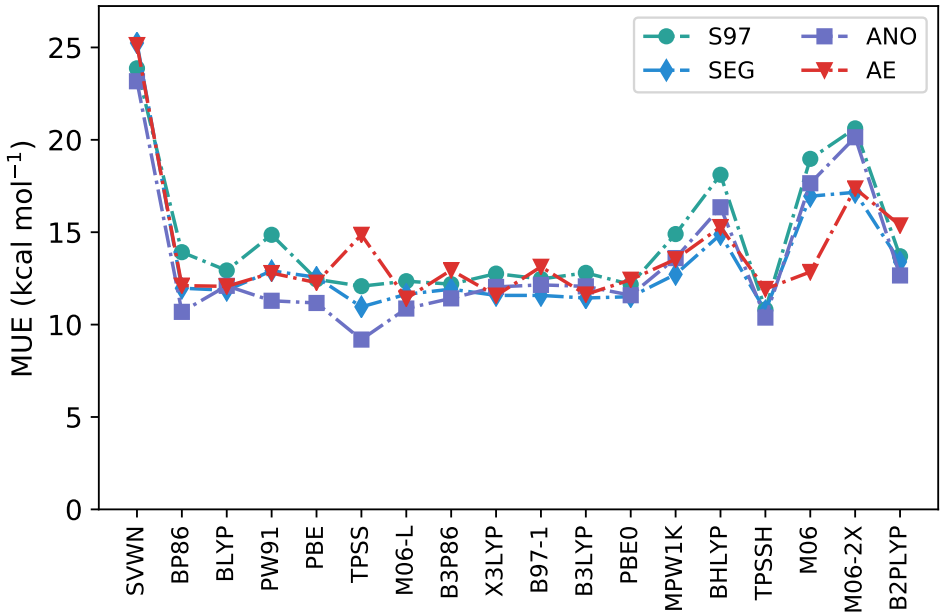

Figure 2: Mean unsigned errors in kcal mol^{-1} for the 18 functionals analyzed across the four basis sets for the overall molecule set.

overestimate or underestimate the experimental values.

For the SEG basis set, the lowest MUE is achieved by TPSSH and TPSS, with values of 10.8 and 11.0 kcal mol^{-1}, respectively, and MSE values of -4.3 and -4.7 kcal mol^{-1}, respectively. The TPSSH value is slightly lower than what was determined using the AE basis set, (11.9 kcal mol^{-1}). However, the TPSS MUE is much lower than the MUE for the AE basis of 14.9 kcal mol^{-1}. The source of the larger MUE for the AE's can be attributed to the uranium compounds, where the MUE for the uranium AE was $\sim$20 kcal mol^{-1}, compared to other compounds where the MUE was $\sim$13 kcal mol^{-1} (Fig. 2).

For the ANO basis sets, the lower MUE is achieved by TPSS and TPSSH with values of 9.2 and 10.4 kcal mol^{-1}, respectively. The MSEs for both however, are -2.4 and -2.8 kcal mol^{-1}, indicating the tendency to equally predict enthalpies that are more positive or more negative than experiment. However, the range of TPSSH is 10 kcal mol^{-1} lower than that of the segmented sets, and the standard deviation is 6.7, which is the lowest SD for any of the functionals when paired with the ANO basis set. Of all the basis sets, the meta-GGAs and

the meta-hybrid TPSSH perform the best, overall, regardless of the choice of basis. Slight improvements in MUE occur in transitioning from AE to SEG to ANO for TPSS and TPSSH. The functionals that do the poorest are those with the highest percentages of exact exchange (>40%), including BHLYP, MPW1K, and M06-2X; or SVWN, the most basic functional.

The reported experimental uncertainties of the NEA and Kovács et al[46] recommended values have been reported at the 95% confidence interval.[46] The average of the uncertainties is approximately 4 kcal mol^{-1}, thus in considering thermochemical accuracy in the computationally predicted energies, any method that can attain a MUE of ∼4 kcal mol^{-1} is of greatest interest.

Spin–Orbit Effects

SO-DFT calculations were performed on the An66 set, using the SEG and ANO basis sets from the Stuttgart RECP family. The summary statistics are reported in Table 2 and in Figure 3, total MUEs and MSEs for DFT and SO-DFT with the SEG and ANO basis are provided. As shown in Figure 3, there seems to be a limited difference between the overall DFT and SO-DFT MUE values in considering the entire set of molecules. However, in closer examination of each actinide, more substantial changes are noted for some of the molecule types. Generally there is an increase in the MSE for SO-DFT, however, the errors relative to experiment are more similar from one molecule to the next than for DFT. In this sense, SO-DFT enhances the functional reliability. In terms of basis sets, TPSSH with the ANO set had the lowest MUE of 9.8 kcal mol^{-1} For the thorium compounds the SO effects were not significant, and for uranium compounds, overall, the SO effects impact the MUE by about ±1 kcal mol^{-1}. For Np, Pu, and Am the effects of SOC are more important, (Fig. 4), as demonstrated by the large reductions to the MUE that occurs for all functionals except SVWN when SO-DFT is used. For the Am compounds, SOC is necessary in order to achieve the lowest MUE for the functionals, with reductions in the MUE ranging from approximately 10-30 kcal mol^{-1}, as shown in Figure 4.

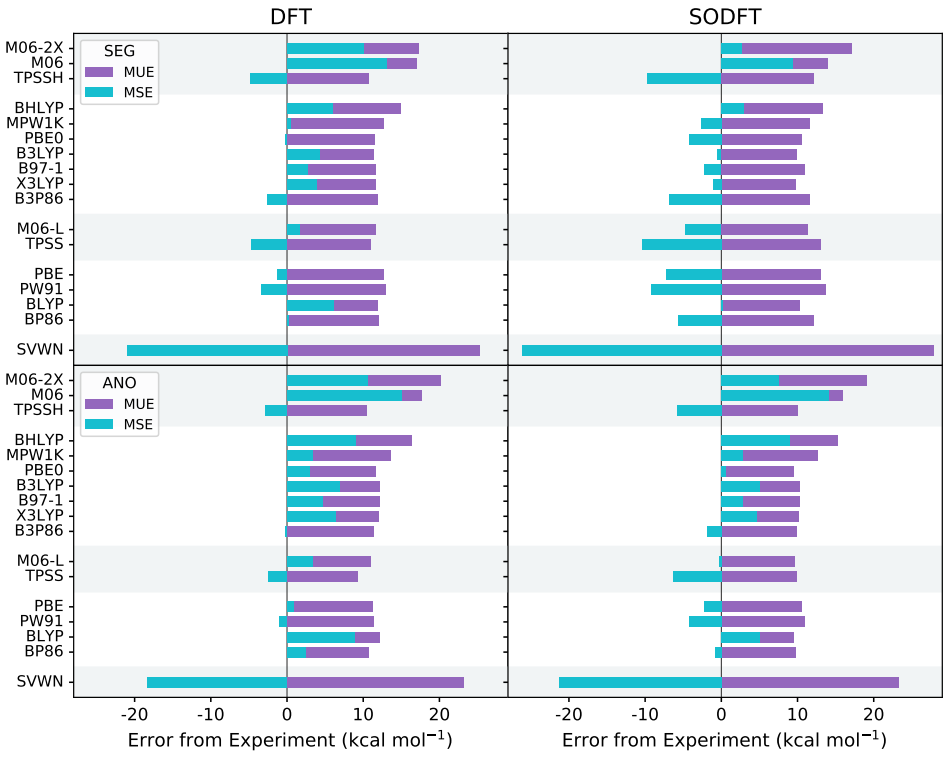

Figure 3: Comparison of the DFT and SO-DFT results for both SEG and ANO bases. MUE bars are shown in purple and the MSE bars are shown in cyan.

Table 2: Statistical properties computed for the enthalpies predicted by each functional at the SO-DFT level, for the SEG and ANO basis sets. Similar to Table 1, the statistics include the mean unsigned error (MUE), mean signed error (MSE), the range of errors noted (Min and Max), all in kcal mol^{-1}, and finally the standard deviation σ.

	MUE		MSE		Min		Max		σ	
	SEG	ANO	SEG	ANO	SEG	ANO	SEG	ANO	SEG	ANO
SVWN	27.9	23.3	−26.2	−21.3	−101.4	−87.5	16.7	18.0	22.9	20.3
BP86	12.1	9.8	−5.7	−0.8	−48.6	−39.6	29.9	32.4	10.7	9.0
BLYP	10.3	9.5	0.2	5.1	−39.2	−25.5	34.7	37.5	9.4	9.4
PW91	13.7	10.9	−9.2	−4.2	−56.3	−45.4	26.2	28.1	12.1	9.9
PBE	13.0	10.5	−7.3	−2.3	−52.2	−42.6	29.1	31.6	11.4	9.5
TPSS	13.0	9.9	−10.4	−6.3	−54.7	−41.2	21.3	20.0	10.7	8.7
M06-L	11.3	9.7	−4.7	−0.3	−47.9	−36.8	28.2	31.5	9.7	9.0
B3P86	11.6	9.9	−6.9	−1.9	−33.0	−18.8	18.4	23.6	6.7	6.3
X3LYP	9.8	10.2	−1.1	4.6	−23.0	−16.8	25.9	37.6	6.3	8.7
B97-1	10.9	10.3	−2.2	2.8	−22.7	−18.7	26.3	32.0	6.7	8.3
B3LYP	9.9	10.3	−0.5	5.0	−22.8	−16.6	26.1	45.4	6.3	9.4
PBE0	10.6	9.5	−4.2	0.6	−23.9	−18.3	24.4	32.2	6.1	7.1
MPW1K	11.6	12.7	−2.7	2.8	−23.8	−19.3	41.0	52.7	8.1	10.3
BHLYP	13.3	15.3	2.9	9.0	−21.5	−17.8	54.6	67.0	12.0	15.7
TPSSH	12.2	10.1	−9.7	−5.8	−42.9	−31.4	19.5	20.4	8.4	7.4
M06	14.0	16.0	9.4	14.1	−20.2	−14.6	41.2	42.8	10.4	10.9
M06-2X	17.1	19.1	2.7	7.6	−36.5	−31.2	67.6	80.8	13.7	17.3

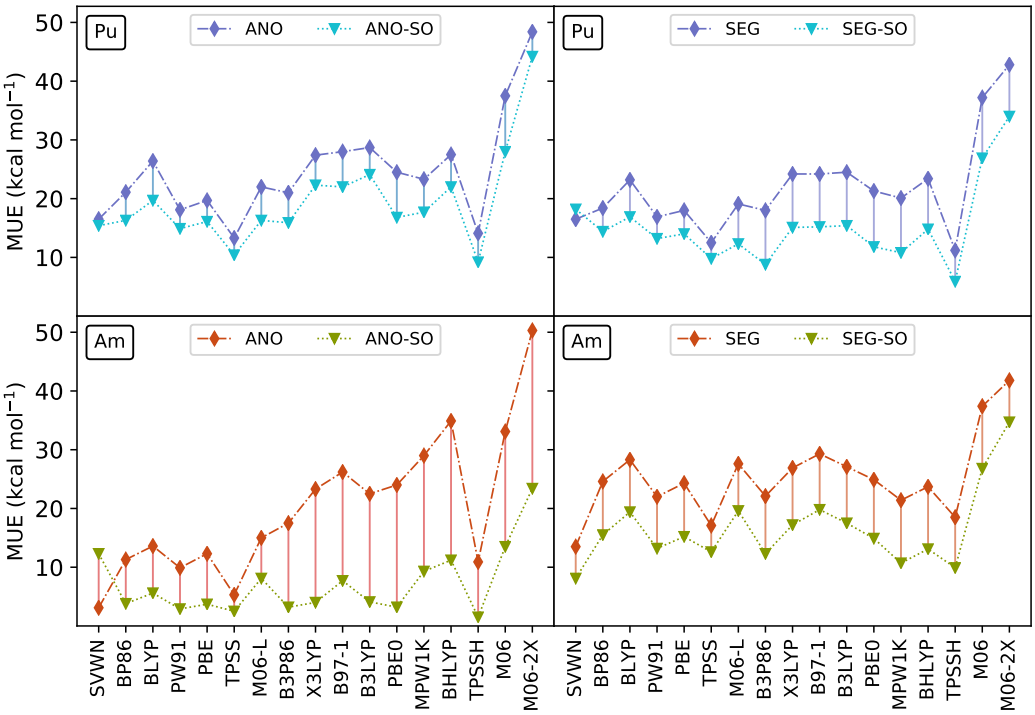

Figure 4: The error reduction of SO-DFT on the later actinides for the SEG and ANO basis.

Regression Analysis

Regression analysis shows the overall consistency, i.e., the distribution of the error and accuracy of the functionals across the wide span of molecules. The combined linear regression tests for all compounds computed with the RECP for the ANO and SEG basis sets with and without SO-DFT are listed in Tables 3 and 4. The experimental enthalpies of formation are compared against the computed enthalpies of formation utilizing a linear fit with least-squares regression:

$$\Delta H_{exp} = m\Delta H_{calc} + b \tag{1}$$

where m is the slope and b the y-intercept. In an ideal situation the slope is 1 and the intercept 0, with a very high R^2 value (> 0.990). A functional is considered consistent if it maintains a high R^2 value from one basis set to the next (e.g., for ANO and then for SEG) while having similar slopes and intercepts. The functionals are ranked in Table 3 by the R^2.

Overall, TPSSH resulted in the highest R^2 values for the AE and SEG basis sets, and the second highest for the ANO basis. The highest R^2 for the ANO basis set was for TPSS with a slope of 0.99354. TPSS had the second highest R^2 value for the SEG basis set, however, for the AE basis set, its ranking was seventh. M06-L had the second highest ranking for the AE basis set, and seventh for the SEG basis. In addition to TPSSH, B3P86 had greater consistency (similar performance) across the basis sets, evidenced by its ranking of third, fifth, and third for AE, SEG, and ANO basis sets, respectively. The lowest scoring functional was M06-2X, which scored last for all three basis sets, with an R^2 of 0.96591 for the AE basis.

For the SO-DFT calculations, the TPSSH functional has the highest R^2 values for both the SEG and ANO basis sets, with values of 0.99460 and 0.99432, respectively. B3P86 ranked second overall for the SEG basis and third for the ANO basis. TPSS ranked second with the ANO basis, but only sixth for the SEG basis. For the R^2 of the SEG basis, TPSS has a value of 0.99208 for DFT, and 0.99299 for SO-DFT. Thus, the accuracy did improve with use of SO-DFT, however, for other functions the improvements were much better. Overall, these results demonstrate the importance of SO-DFT for most functionals.

In considering aspects beyond how well the data fits a linear trend, the intercepts should be considered. For example, for the ANO basis, TPSSH had a slope of 0.999 and an intercept of -3.0 for DFT and a slope of 1.004 and intercept of -5.2 for SO-DFT. The negative y-intercept suggests an additive systematic deviation, i.e., all values are shifted from experiment by about -5.2 kcal mol^{-1}. This implies that, considering this shift, a direct comparison with experiment and TPSSH values can, at the very least, provide qualitative trends.

Table 3: Linear regression analysis information for each functional at the two DFT/RECP levels of theory and the DFT/AE level of theory. A rank is given based on the overall R^2 in comparison to other functionals. In the table x is used to represent ΔH_{exp}.

	R^2			$\Delta H_{exp} = m\Delta H_{calc} + b$			Rank		
	AE	SEG	ANO	AE	SEG	ANO	AE	SEG	ANO
SVWN	0.98123	0.98048	0.98250	$1.081x - 9.5$	$1.078x - 9.4$	$1.080x - 6.5$	16	17	16
BP86	0.98861	0.98867	0.99069	$1.012x + 1.0$	$1.003x + 0.7$	$1.004x + 3.0$	10	10	6
BLYP	0.98917	0.98942	0.99108	$1.005x + 6.0$	$0.995x + 5.4$	$0.995x + 8.0$	8	9	4
PW91	0.98858	0.98833	0.99012	$1.023x - 1.3$	$1.014x - 1.2$	$1.013x + 1.0$	11	12	7
PBE	0.98845	0.98803	0.98989	$1.017x - 0.1$	$1.008x - 0.1$	$1.007x + 2.0$	12	14	8
TPSS	0.98924	0.99208	0.99354	$1.018x - 6.4$	$1.010x - 3.2$	$1.007x - 1.4$	7	2	1
M06-L	0.99159	0.99006	0.99119	$1.018x - 0.2$	$1.014x + 3.8$	$1.012x + 5.1$	2	7	3
B3P86	0.99037	0.99121	0.99097	$1.010x - 2.5$	$0.993x - 3.6$	$0.996x - 0.9$	3	3	5
X3LYP	0.99018	0.99049	0.98982	$1.001x + 2.8$	$0.983x + 1.3$	$0.985x + 4.2$	4	5	9
B97-1	0.98793	0.99003	0.98880	$0.995x + 0.8$	$0.983x + 0.2$	$0.986x + 2.6$	13	8	12
B3LYP	0.99007	0.99067	0.98968	$0.997x + 2.3$	$0.981x + 1.5$	$0.985x + 4.6$	5	4	10
PBE0	0.98970	0.99044	0.98954	$1.000x - 1.5$	$0.982x - 2.9$	$0.987x + 1.0$	6	6	11
MPW1K	0.98634	0.98826	0.98494	$0.998x - 1.0$	$0.973x - 3.5$	$0.978x + 0.1$	14	13	15
BHLYP	0.97998	0.98332	0.97868	$0.993x + 4.4$	$0.967x + 1.0$	$0.973x + 4.9$	17	16	17
TPSSH	0.99245	0.99332	0.99328	$1.008x - 5.2$	$0.996x - 5.3$	$0.999x - 3.0$	1	1	2
M06	0.98907	0.98521	0.98631	$1.009x + 7.3$	$0.980x + 10$	$0.985x + 13$	9	15	14
M06-2X	0.97449	0.97537	0.96591	$0.996x + 10$	$0.958x + 3.8$	$0.966x + 5.4$	18	18	18
B2PLYP	0.98538	0.98867	0.98799	$1.037x + 1.0$	$1.010x - 1.1$	$1.010x + 2.6$	15	11	13

Table 4: Linear regression analysis information for each functional at the SO-DFT levels of theory and the DFT/AE level of theory. A rank is given based on the overall R^2 in comparison to other functionals. In the table x is used to represent ΔH_{exp}.

	R^2		$\Delta H_{exp} = m\Delta H_{calc} + b$		Rank	
	SEG	ANO	SEG	ANO	SEG	ANO
SVWN	0.98294	0.98574	$1.090x - 12.9$	$1.080x - 9.5$	16	15
BP86	0.99017	0.99197	$1.019x - 2.8$	$1.008x + 0.3$	11	10
BLYP	0.99120	0.99294	$1.010x + 1.7$	$0.999x + 4.9$	9	5
PW91	0.98988	0.99147	$1.030x - 4.7$	$1.019x - 1.4$	13	12
PBE	0.98969	0.99129	$1.024x - 3.6$	$1.013x - 0.4$	14	13
TPSS	0.99299	0.99407	$1.028x - 6.2$	$1.011x - 4.7$	6	2
M06-L	0.99219	0.99225	$1.031x - 0.1$	$1.014x + 1.8$	8	7
B3P86	0.99411	0.99371	$1.012x - 5.1$	$0.998x - 2.2$	2	3
X3LYP	0.99376	0.99260	$1.000x - 1.1$	$0.988x + 2.9$	4	6
B97-1	0.99270	0.99218	$1.003x - 1.9$	$0.989x + 1.2$	7	8
B3LYP	0.99358	0.99215	$1.001x - 0.3$	$0.988x + 3.2$	5	9
PBE0	0.99385	0.99345	$1.000x - 4.1$	$0.989x - 1.0$	3	4
MPW1K	0.99098	0.98797	$0.990x - 4.3$	$0.974x - 1.0$	10	14
BHLYP	0.98548	0.98156	$0.984x + 0.5$	$0.969x + 4.4$	15	16
TPSSH	0.99460	0.99432	$1.018x - 7.1$	$1.004x - 5.2$	1	1
M06	0.99004	0.99189	$0.998x + 9.1$	$0.987x + 12.2$	12	11
M06-2X	0.97804	0.97162	$0.985x + 0.4$	$0.966x + 2.5$	17	17

Summary

In conclusion, a study of the enthalpies of formation computed by a variety of DFT functionals for different basis sets and the impact of SOC effects on the predictions is presented. In prior work on lanthanides, the AE approaches resulted in much lower MUEs than the RECP's,[7,9] whereas in this study, not only are the differences not as pronounced, but, AE's do not always result in the lower MUEs. In fact, the analysis shows the AE and RECP basis sets result in enthalpies of formation with differences usually within ∼2-3 kcal mol^{-1} of one another, though largely for Np, Pu, and Am, there are a number of functionals that result in differences of ∼5-10 kcal mol^{-1}, depending upon functional. The closer overall performance between AE's and RECP's is useful, as RECP's are much more computationally efficient, which is particularly important, considering the cost of the DKH method.

In the earlier lanthanide study, SVWN resulted in the lowest MUE in most cases and gave

very consistent deviations from experiment. The performance for the actinides was similar for SVWN itself, but for the other functionals, significant improvements were shown for many of the molecules with MUEs of $\sim$10 kcal mol^{-1}, even without the inclusion of SOC which his less than half the errors encountered for lanthanides, overall. With that said, the lanthanide studies differed in a number of key ways: the availability of experimental data allowed the entire series to be detailed for lanthanides, which was not possible for the actinides. It is established that lanthanide bonding, is overall, more ionic in nature than early actinide bonding. As such, it is not surprising that there is substantial improvement (though still not ideal) for actinides, with performance that is more akin to that of transition metals. For future actinide studies utilizing DFT, this study suggests that TPSS and TPSSH are among the better functionals for the computation of thermochemical energies. Given, the degrading performance for B3LYP, BP86, PBE, and PBE0 for actinides beyond uranium, reliance on these functionals is not recommended.

There is a stark increase in error for the Pu compounds for almost all of the functionals in comparison to the other actinide compounds. However, the most consistent errors in terms of MUE, are produced by TPSSH, where little difference in the MUE is seen among each group of actinides. This is demonstrated by the linear regression results, where TPSSH was the most consistent across all the compounds for RECP and AE. For the Np, Pu, and Am compounds, there is a deterioration of performance for the more parameterized functionals and those with higher percentages of exact exchange.

Supporting Information Available

Supporting Information is available for free on the ACS Publications website.

DFT-based enthalpies of formation and total energies for the An66 molecules for each density functional and basis set combination; experimental values and associated uncertainties for the An66 molecule set; optimized TPSS geometries for each An66 molecule along with

the thermokinetic constants and multiplicities used.

Acknowledgement

This material is based upon work supported by the National Science Foundation under Grant no. CHE-1900086. This work also utilized computational facilities at the Center for Advanced Scientific Computing and Modeling (CASCaM) at the University of North Texas, which, in part, was supported by NSF Grant No. CHE-1531468, as well as the Institute for Cyber-Enabled Research (ICER) at Michigan State University.

References

(1) Pahan, S.; Boda, A.; Ali, S. M. Density functional theoretical analysis of structure, bonding, interaction and thermodynamic selectivity of hexavalent uranium (UO_2^{2+}) and tetravalent plutonium (Pu^{4+}) ion complexes of tetramethyl diglycolamide (TM). *Theor. Chem. Acc.* **2015**, *134*, 1–16.

(2) Kovács, A.; Konings, R. J. M.; Gibson, J. K.; Infante, I.; Gagliardi, L. Quantum chemical calculations and experimental investigations of molecular actinide oxides. *Chem. Rev.* **2015**, *115*, 1725–1759.

(3) Gelis, A. V.; Lumetta, G. J. Actinide lanthanide separation process - ALSEP. *Ind. Eng. Chem. Res.* **2014**, *53*, 1624–1631.

(4) Eliav, E.; Kaldor, U. In *Comput. Methods Lanthan. Actin. Chem.*, 1st ed.; Dolg, M., Ed.; 2015; Chapter 2, pp 23–54.

(5) Cao, Z.; Dolg, M. *Relativistic Methods for Chemists*; Springer: Berlin, 2009; p 37.

(6) Karton, A.; Daon, S.; Martin, J. M. L. W4-11: A high-confidence benchmark dataset

for computational thermochemistry derived from first-principles W4 data. *Chem. Phys. Lett.* **2011**, *510*, 165–178.

(7) Aebersold, L. E.; Yuwono, S. H.; Schoendorff, G.; Wilson, A. K. Efficacy of Density Functionals and Relativistic Effective Core Potentials for Lanthanide-Containing Species: The Ln54 Molecule Set. *J. Chem. Theory Comput.* **2017**, *13*, 2831–2839.

(8) DeYonker, N. J.; Cundari, T. R.; Wilson, A. K. The correlation consistent composite approach (ccCA): An alternative to the Gaussian-n methods. *J. Chem. Phys.* **2006**, *124*.

(9) Grimmel, S.; Schoendorff, G.; Wilson, A. K. Gauging the Performance of Density Functionals for Lanthanide-Containing Molecules. *J. Chem. Theory Comput.* **2016**, *12*, 1259–1266.

(10) Slater, J. C.; Johnson, K. H. Self-consistent-field cluster method for polyatomic molecules and solids. *Phys. Rev. B* **1972**, *5*, 844.

(11) Vosko, S. H.; Wilk, L.; Nusair, M. Accurate spin-dependent electron liquid correlation energies for local spin density calculations: a critical analysis. *Can. J. Phys.* **1980**, *58*, 1200–1211.

(12) Becke, A. D. Density-Functional Exchange-Energy Approximation with Corrects Asymptotic-Behavior. *Phys. Rev. A* **1988**, *38*, 3098–3100.

(13) Perdew, J. P. Density-functional approximation for the correlation energy of the inhomogeneous electron gas. *Phys. Rev. B* **1986**, *33*, 8822–8824.

(14) Lee, C.; Yang, W.; Parr, R. G. Development of the Colle-Salvetti correlation-energy formula into a functional of the electron density. *Phys. Rev. B* **1988**, *37*, 785–789.

(15) Perdew, J. P. In *Electron. Struct. Solids '91*; Ziesche, P., Eschrig, H., Eds.; Akademie Verlag: Berlin, 1991; p 11.

(16) Perdew, J. P.; Burke, K.; Ernzerhof, M. Generalized Gradient Approximation Made Simple. *Phys. Rev. Lett.* **1996**, *77*, 3865–3868.

(17) Tao, J.; Perdew, J. P.; Staroverov, V. N.; Scuseria, G. E. Climbing the density functional ladder: nonempirical meta-generalized gradient approximation designed for molecules and solids. *Phys. Rev. Lett.* **2003**, *91*, 146401.

(18) Zhao, Y.; Truhlar, D. G. A new local density functional for main-group thermochemistry, transition metal bonding, thermochemical kinetics, and noncovalent interactions. *J. Chem. Phys.* **2006**, *125*, 194101.

(19) Becke, A. D. A new mixing of Hartree–Fock and local density-functional theories. *J. Chem. Phys.* **1993**, *98*, 1372.

(20) Becke, A. D. Density-functional thermochemistry. V. Systematic optimization of exchange-correlation functionals. *J. Chem. Phys.* **1997**, *107*, 8554.

(21) Hamprecht, F. A.; Cohen, A. J.; Tozer, D. J.; Handy, N. C. Development and assessment of new exchange-correlation functionals. *J. Chem. Phys.* **1998**, *109*, 6264.

(22) Adamo, C.; Barone, V. Toward reliable density functional methods without adjustable parameters: The PBE0 model. *J. Chem. Phys.* **1999**, *110*, 6158.

(23) Lynch, B. J.; Fast, P. L.; Harris, M.; Truhlar, D. G. Adiabatic Connection for Kinetics. *J. Phys. Chem. A* **2000**, *104*, 4811–4815.

(24) Staroverov, V. N.; Scuseria, G. E.; Tao, J. M.; Perdew, J. P. Comparative assessment of a new nonempirical density functional: Molecules and hydrogen-bonded complexes. *J. Chem. Phys.* **2004**, *121*, 11507.

(25) Zhao, Y.; Truhlar, D. G. The M06 suite of density functionals for main group thermochemistry, thermochemical kinetics, noncovalent interactions, excited states, and

transition elements: two new functionals and systematic testing of four M06-class functionals and 12 other function. *Theor. Chem. Acc.* **2008**, *120*, 215–241.

(26) Grimme, S. Semiempirical GGA-type density functional constructed with a long-range dispersion correction. *J. Comput. Chem.* **2006**, *27*, 1787–1799.

(27) Møller, C.; Plesset, M. S. Note on an Approximation Treatment for Many-Electron Systems. *Phys. Rev.* **1934**, *46*, 618–622.

(28) Valiev, M.; Bylaska, E. J.; Govind, N.; Kowalski, K.; Straatsma, T. P.; Van Dam, H. J. J.; Wang, D.; Nieplocha, J.; Apra, E.; Windus, T. L. et al. NWChem: A comprehensive and scalable open-source solution for large scale molecular simulations. *Comput. Phys. Commun.* **2010**, *181*, 1477–1489.

(29) Küchle, W.; Dolg, M.; Stoll, H.; Preuss, H. Energy-adjusted pseudopotentials for the actinides. Parameter sets and test calculations for thorium and thorium monoxide. *J. Chem. Phys.* **1994**, *100*, 7535–7542.

(30) Cao, X.; Dolg, M.; Stoll, H. Valence basis sets for relativistic energy-consistent small-core actinide pseudopotentials. *J. Chem. Phys.* **2003**, *118*, 487–496.

(31) Bergner, A.; Dolg, M.; Küchle, W.; Stoll, H.; Preuß, H. Ab initio energy-adjusted pseudopotentials for elements of groups 13-17. *Mol. Phys.* **1993**, *80*, 1431–1441.

(32) Cao, X.; Dolg, M. Segmented contraction scheme for small-core actinide pseudopotential basis sets. *J. Mol. Struct. THEOCHEM* **2004**, *673*, 203–209.

(33) Dunning, T. H. Gaussian basis sets for use in correlated molecular calculations. I. The atoms boron through neon and hydrogen. *J. Chem. Phys.* **1989**, *90*, 1007–1023.

(34) Dunning T.H., J.; Peterson, K. A.; Wilson, A. K. Gaussian basis sets for use in correlated molecular calculations. X. The atoms aluminum through argon revisited. *J. Chem. Phys.* **2001**, *114*, 9244–9253.

(35) Peterson, K. A. Systematically convergent basis sets with relativistic pseudopotentials. I. Correlation consistent basis sets for the post-d group 13-15 elements. *J. Chem. Phys.* **2003**, *119*, 11099–11112.

(36) Jensen, K. P.; Cirera, J. Accurate computed enthalpies of spin crossover in iron and cobalt complexes. *J. Phys. Chem. A* **2009**, *113*, 10033–10039.

(37) Nakajima, T.; Hirao, K. The higher-order Douglas–Kroll transformation. *J. Chem. Phys.* **2000**, *113*, 7786–7789.

(38) De Jong, W. A.; Harrison, R. J.; Dixon, D. A. Parallel Douglas-Kroll energy and gradients in NWChem: Estimating scalar relativistic effects using Douglas-Kroll contracted basis sets. *J. Chem. Phys.* **2001**, *114*, 48–53.

(39) Peterson, K. A. Correlation consistent basis sets for actinides. I. the Th and U atoms. *J. Chem. Phys.* **2015**, *142*, 074105.

(40) Feng, R.; Peterson, K. A. Correlation consistent basis sets for actinides. II. the atoms Ac and Np-Lr. *J. Chem. Phys.* **2017**, *147*, 084108.

(41) Nakajima, T.; Hirao, K. Extended Douglas–Kroll transformations applied to the relativistic many-electron Hamiltonian. *J. Chem. Phys.* **2003**, *119*, 4105–4111.

(42) Bross, D. H.; Peterson, K. A. Correlation consistent, douglas-kroll-hess relativistic basis sets for the 5p and 6p elements. *Theor. Chem. Acc.* **2014**, *133*, 1–12.

(43) Hong, G.; Dolg, M.; Li, L. A comparison of scalar-relativistic ZORA and DKH density functional schemes: Monohydrides, monooxides and monofluorides of La, Lu, Ac and Lr. *Chem. Phys. Lett.* **2001**, *334*, 396–402.

(44) Guillaumont, R.; Fanghänel, T.; Fuger, J.; Palmer, D. A.; Grenthe, I.; Rand, M.; Mompean, F. J.; Illemassene, M.; Domenech-Orti, C.; Said, K. B. *Update on the Chemical*

Thermodynamics of Uranium, Neptiunium, Plutonium, Americium, and Technitium; OECD Publications: Paris, 2003; Vol. 5.

(45) Rand, M. H.; Fuger, J.; Grenthe, I.; Neck, V.; Rai, D. *Chemical Thermodynamics of Thorium. OECD Nuclear Energy Agency Data Bank - Chemical Thermodynamics*; OECD Publications: Paris, 2008; Vol. 11.

(46) Konings, R. J.; Beneš, O.; Kovács, A.; Manara, D.; Sedmidubskỳ, D.; Gorokhov, L.; Iorish, V. S.; Yungman, V.; Shenyavskaya, E.; Osina, E. The Thermodynamic Properties of the f-Elements and their Compounds: Part 2. The Lanthanide and Actinide Oxides. *J. Phys. Chem. Ref. Data* **2014**, *43*, 013101.

(47) Boguslawski, K.; Réal, F.; Tecmer, P.; Duperrouzel, C.; Gomes, A. S. P.; Legeza, Ö.; Ayers, P. W.; Vallet, V. On the multireference nature of plutonium oxides: $PuO_2{}^{2+}$, PuO_2, PuO_3 and $PuO_2(OH)_2$. *Phys. Chem. Chem. Phys.* **2017**, *19*, 4317–4329.

(48) Pereira Gomes, A. S.; Réal, F.; Galland, N.; Angeli, C.; Cimiraglia, R.; Vallet, V. Electronic structure investigation of the evanescent AtO+ ion. *Phys. Chem. Chem. Phys.* **2014**, *16*, 9238–9248.

TOC Graphic

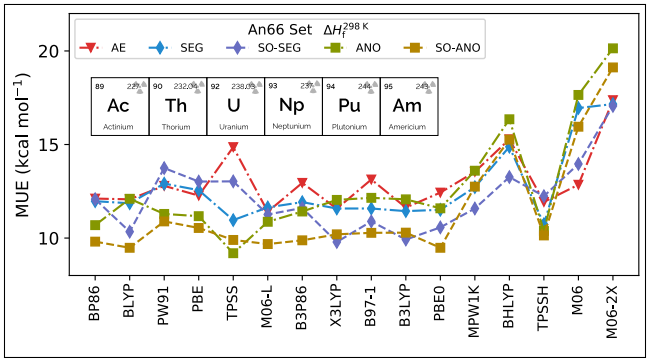
An66 Set $\Delta H_f^{298\,K}$
AE
SEG
SO-SEG
ANO
SO-ANO
MUE (kcal mol^{-1})
20
15
10
89 Ac Actinium
90 Th Thorium
92 U Uranium
93 Np Neptunium
94 Pu Plutonium
95 Am Americium
BP86
BLYP
PW91
PBE
TPSS
M06-L
B3P86
X3LYP
B97-1
B3LYP
PBE0
MPW1K
BHLYP
TPSSH
M06
M06-2X